ATLAS CONF Note

ATLAS-CONF-2020-052

29th October 2020

Combination of searches for invisible Higgs boson decays with the ATLAS experiment

The ATLAS Collaboration

Many extensions of the Standard Model predict the production of dark matter particles at the LHC. Sufficiently light dark matter particles may be produced in decays of the Higgs boson H that would appear invisible to the detector. This document presents a statistical combination of searches for $H \rightarrow$ invisible decays where the H is produced according to the Standard Model via vector boson fusion or in association with a pair of top quarks in final states with zero or two leptons. These searches are performed with the ATLAS detector using 139 fb^{-1} of pp collisions at a centre-of-mass energy of $\sqrt{s} = 13$ TeV at the LHC. In combination with the results at $\sqrt{s} = 7$ and 8 TeV, an upper limit on the $H \rightarrow$ invisible branching ratio of 0.11 ($0.11^{+0.04}_{-0.03}$) at 95% confidence level is observed (expected). These results are also interpreted in the context of models where the 125 GeV Higgs boson acts as a portal to dark matter, and limits are set on the scattering cross-section of weakly interacting massive particles and nucleons.

ATLAS-CONF-2020-052
29 October 2020

1 Introduction

One of the central open questions in physics today is the nature of dark matter (DM) that is found to comprise the majority of the matter in the universe [1–4]. A compelling candidate for DM is a stable, electrically neutral particle χ whose non-gravitational interactions with Standard Model (SM) particles are weak. Such a particle with a mass comparable to the mass scale of the electroweak-sector particles could be detectable [5–7] and accommodate the observed DM relic density [8, 9]. Numerous models predict observable production rates of such DM particles at the Large Hadron Collider (LHC) [10–12]. In a wide class of those models, the 125 GeV Higgs boson H [13, 14] acts as a portal between a dark sector and the SM sector, either through Yukawa-type couplings to fermionic dark matter, or other mechanisms [15–28]. If kinematically allowed, decays of the Higgs boson to DM particles represent a distinct signature in such models. Higgs boson decays to DM particles can only be indirectly inferred through missing transverse momentum[1] $E_{\mathrm{T}}^{\mathrm{miss}}$ due to DM particles escaping detection, and are therefore termed "invisible" (inv). In the SM, the invisible Higgs boson branching ratio $\mathcal{B}_{H\to\mathrm{inv}}$ is 0.1% from $H \to ZZ^* \to 4\nu$ decays [29].

Direct searches for invisible Higgs boson decays were carried out with the ATLAS detector [30–32] using up to 4.7 fb^{-1}of pp collision data delivered by the LHC in 2011 at a center-of-mass energy of $\sqrt{s}$ = 7 TeV and 20.3 fb^{-1}at 8 TeV in 2012, collectively known as Run 1. Different event topologies were considered, assuming SM production rates: vector boson fusion (VBF) [33], Higgsstrahlung from a Z boson decaying into a pair of electrons or muons (Z(lep)H) [34], and Higgsstrahlung from a W or Z boson decaying into hadrons (V(had)H) [35]. These searches for invisible Higgs boson decays were statistically combined, and an upper limit at the 95% confidence level (CL) of $\mathcal{B}_{H\to\mathrm{inv}} < 0.25\ (0.27^{+0.10}_{-0.08})$ [36] was observed (expected). In combination with measurements of visible decay modes of the Higgs boson using an effective field theory framework ("κ-framework") where the assumption that the Higgs boson is produced according to the SM is dropped, the observed (expected) upper limit improved to 0.23 (0.24) [36]. Direct searches for invisible Higgs boson decays were performed using pp collision data at $\sqrt{s}$ = 13 TeV recorded at the LHC during 2015 and 2016 in the VBF [37], Z(lep)H [38], and V(had)H [39] topologies with the ATLAS detector. The results of these searches were statistically combined [40], including Run 1 results, providing an upper limit of $\mathcal{B}_{H\to\mathrm{inv}} < 0.26\ (0.17^{+0.07}_{-0.05})$ at the 95% CL. In combination with visible decay modes of the Higgs boson using the κ-framework, the observed (expected) upper limit changed to 0.30 (0.16) [41]. More recently, searches using the full Run 2 data of up to 139 fb^{-1} were performed in the VBF [42] and gluon fusion [43] topologies. Also the $t\bar{t}H$ topology, where the Higgs boson is produced in association with two top quarks, was explored by analysing final states with 0 [44], 1 [45], and 2 leptons [46] from the decay of the $t\bar{t}$ system. The most recent result in the VBF topology has been combined with visible decay modes of the Higgs boson using the κ-framework, and the observed (expected) upper limit improved to 0.09 (0.11) [47]. Similar searches were performed by the CMS Collaboration [48–54].

This document presents the statistical combination of the Run 2 searches for invisible decays of the Higgs boson in the VBF and $t\bar{t}H$ topologies, where the latter is a reinterpretation of searches for new phenomena in association with heavy flavour quarks and encompasses final states with two leptons ($t\bar{t}H$-2ℓ) and without any leptons ($t\bar{t}H$-0ℓ). These searches all use 139 fb^{-1} of data and will be referred to as "Run 2 results" in the following. Subsequently, a statistical combination with the combined Run 1 result [36] from the

[1] ATLAS uses a right-handed coordinate system with its origin at the nominal interaction point (IP) in the centre of the detector and the z-axis along the beam pipe. The x-axis points to the centre of the LHC ring, and the y-axis points upward. Cylindrical coordinates (r, ϕ) are used in the transverse plane, ϕ being the azimuthal angle around the z-axis. The pseudorapidity is defined in terms of the polar angle θ as $\eta = -\ln\tan(\theta/2)$. The distance between two objects in η–ϕ space is $\Delta R = \sqrt{(\Delta\eta)^2 + (\Delta\phi)^2}$. Transverse momentum is defined by $p_{\mathrm{T}} = p\sin\theta$.

ATLAS collaboration is performed. The analysis is performed under the assumption of SM Higgs boson production. Visible decay modes of the Higgs boson are not considered.

The analysed pp collision data was recorded with the ATLAS detector [30, 31], a multi-purpose particle detector with a forward-backward symmetric cylindrical geometry and nearly full coverage in solid angle. It consists of an inner tracking detector surrounded by a thin superconducting solenoid providing a 2 T axial magnetic field, electromagnetic and hadron calorimeters, and a muon spectrometer.

2 Individual searches

The following inputs are considered for the combination:

1. search for invisible decays of the Higgs boson in the VBF topology [42]
2. search for invisible decays of the Higgs boson in the $t\bar{t}H$ topology in the 0ℓ and 2ℓ channels [44, 46]
3. Run 1 combination [36]

A brief overview of the analyses is given below. By construction, there is no overlap between the events selected for the VBF and the $t\bar{t}H$ topologies. The overlap between the $t\bar{t}H$-0ℓ and $t\bar{t}H$-2ℓ analyses in the $t\bar{t}H$ topology is discussed below.

2.1 VBF topology

In the VBF topology, the $H \rightarrow$ inv signal is characterised by two jets with a wide separation in pseudorapidity and missing energy from the invisible Higgs decay. The analysis targeting this signature selects events collected with the $E_{\mathrm{T}}^{\mathrm{miss}}$ trigger and requires $E_{\mathrm{T}}^{\mathrm{miss}} > 200$ GeV to suppress the multijet background. Events are further selected if they contain two, three or four jets with $p_{\mathrm{T}} > 25$ GeV, with the two with the highest p_{T} fulfilling the VBF requirements: lying in opposite longitudinal hemispheres, being well separated in η and not back-to-back in the transverse plane. In order to reduce the contribution from V+jets and $t\bar{t}$ production and to ensure orthogonality with the other analyses, events with lepton or photon candidates are vetoed, as are those which contain two or more jets identified as containing b-hadrons (b-tagged jets). Final discrimination is obtained by splitting events with either 3 or 4 jets and exactly two jets in two categories and, for the events in the latter, binning the $(m_{jj}, \Delta\phi_{jj})$ plane into five m_{jj} and two $\Delta\phi_{jj}$ regions. In this signature, the dominant background sources are $Z(\nu\nu)$ + jets and $W(\ell\nu)$ + jets production, where the charged lepton ℓ is not detected. Control regions (CR) enriched in $Z(\ell\ell)$ + jets and $W(\ell\nu)$ + jets processes with $\ell = e, \mu$ are defined to constrain the Monte Carlo (MC) simulation normalisation, while the multijet background is directly estimated from data.

This analysis observes (expects) an upper limit on $\mathcal{B}_{H\rightarrow\mathrm{inv}}$ of 0.13 ($0.13^{+0.05}_{-0.04}$) at the 95% CL.

2.2 $t\bar{t}H$ topology

The production mode of the Higgs boson in association with top-quark pairs is targeted by reinterpreting two searches for new phenomena in association with heavy flavour quarks. The final states arising from this production mode are characterised by the presence of b-tagged jets and different charged lepton multiplicities, depending on the decay mode of the two W bosons from the $t\bar{t}$ decays, in addition to $E_{\mathrm{T}}^{\mathrm{miss}}$ coming from the invisible decay products of the Higgs boson and from neutrinos.

The first analysis [44] targeting the $t\bar{t}H$ topology is optimised to search for scalar partners of the top quark (top squarks) and considers the all-hadronic decay mode of the $t\bar{t}$ system by selecting events collected with the $E_{\mathrm{T}}^{\mathrm{miss}}$ trigger with no reconstructed leptons. Furthermore, the presence of at least two b-tagged jets and $E_{\mathrm{T}}^{\mathrm{miss}} > 250$ GeV, to attain full trigger efficiency, are required. Four signal regions (SR) are then defined to address different kinematic regions depending on the mass spectrum of the supersymmetric particles considered. Only the two orthogonal regions designed to address two-body top-squark decays are considered for this $H \to$ inv interpretation. Each of these regions is broken down further into three, defined by the mass of the reclustered large-radius ($R = 1.2$) jet of the sub-leading top quark candidate, $m_2^{R=1.2}$, with divisions at 60 and 120 GeV. Figure 1 (a) shows the leading reclustered jet mass distribution for the events selected in the most sensitive SR to the $t\bar{t}H$ signal. The dominant background process is Z+heavy-flavour jets, but there is also contribution from W+jets, $t\bar{t}Z$, $t\bar{t}$, and single-top Wt. These background sources are modelled with MC simulations and constrained in CRs enhanced in each particular background component.

The second analysis [46] is a search for new physics in events with two opposite-charge leptons (electrons or muons), jets and missing transverse momentum, exploiting events collected with dilepton triggers. The event selection is designed specifically to address DM models in which a spin-0 mediator particle (here the SM Higgs boson) is created in association with $t\bar{t}$ and couples directly to DM. Events are required to have at least one b-tagged jet and an $E_{\mathrm{T}}^{\mathrm{miss}}$-significance greater than 12, which is computed from the expected resolutions for all the objects used in the $E_{\mathrm{T}}^{\mathrm{miss}}$ calculation [55]. Events are then further split depending on whether the two leptons have the same or different flavour, and in the same-flavour selection the additional requirement of $|m_{\ell\ell} - m_Z| > 20$ GeV is added to suppress the Z+jets background. In this selection, the main discriminating variable is the stransverse mass m_{T2} [56, 57], which is used to bound the individual masses of a pair of particles that are each presumed to have decayed into one visible and one invisible particle, calculated using the two leptons as visible particles. To maximise the search sensitivity, the m_{T2} spectrum is divided into six bins, starting from 110 GeV. The m_{T2} distribution for events selected with two leptons with the same flavour is presented in Figure 1 (b). In this search, the main backgrounds are $t\bar{t}$, $t\bar{t}Z$, single-top in the tW channel, Z/γ^*+jets, and diboson processes. Those backgrounds are estimated with MC simulations, while the background from fake/non-prompt leptons is estimated in a data-derived way. Orthogonal CRs are defined to constrain with data the dominant contributions: $t\bar{t}$ and $t\bar{t}Z$.

While the SRs are disjoint, an overlap is observed in the two searches, between the CRs defined to constrain the $t\bar{t}Z$ background. For this process, both analyses adopted a similar strategy and constrained the $t\bar{t}Z$ (with $Z \to \nu\nu$) populating their SRs, with events with three leptons where the purity of $t\bar{t}Z$ (with $Z \to \ell\ell$) is maximised. In the combination, the $t\bar{t}Z$ estimation is harmonised: only the high-statistics $t\bar{t}Z$-CR from the $t\bar{t}H$-2ℓ analysis is used. An additional uncertainty of 24% on the $t\bar{t}Z$ yield in the $t\bar{t}H$-0ℓ analysis is included that accounts for the difference in the $t\bar{t}Z$ normalisation when considering the two different CR definitions, and covers for the larger extrapolation from the $t\bar{t}Z$-CR to the $t\bar{t}H$-0ℓ SR.

When interpreting the analyses as $H \to$ inv searches, the individual observed (expected) limits on

$\mathcal{B}_{H\to\text{inv}}$ at the 95% CL in the $t\bar{t}H$-0ℓ and in the $t\bar{t}H$-2ℓ channels are 0.94 ($0.64^{+0.29}_{-0.19}$) and 0.37 ($0.42^{+0.19}_{-0.12}$), respectively.

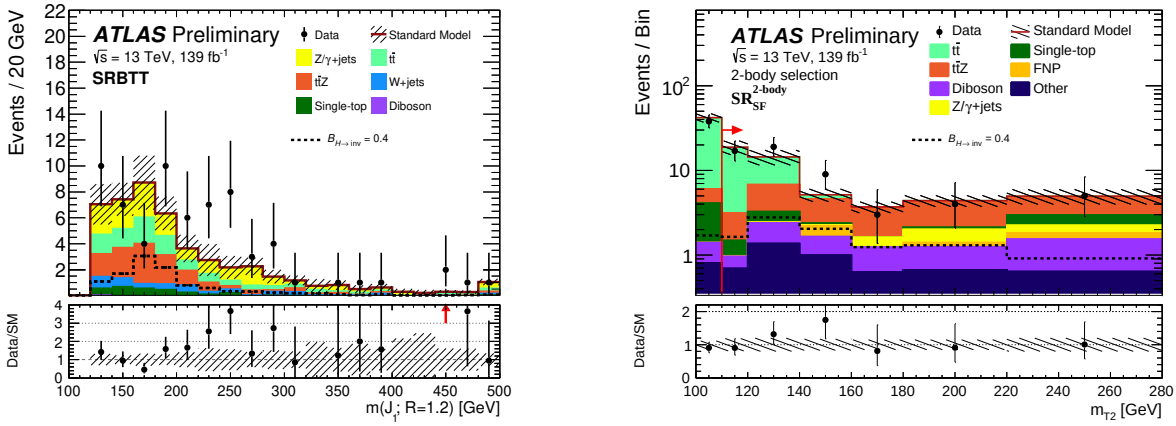

(a) (b)

Figure 1: Distribution of the invariant mass of the leading reclustered jet $m_1^{R=1.2}$ representing the leading top quark candidate in the most sensitive "SRBTT" region of the $t\bar{t}H$-0ℓ channel (a). The SRBTT region is characterised by $m_{\text{T2}} < 450$ GeV and requires, among other selections, the sub-leading top quark candidate to have $m_2^{R=1.2} > 120$ GeV. The m_{T2} distribution for the same-flavour events selected in the $t\bar{t}H$-2ℓ channel (b). The contributions from all the backgrounds are shown as stacked histograms, with the hatched bands representing the total uncertainty. The expected distributions for the $H \to$ inv signal are overlaid as dashed lines. Red arrows in the ratio panel indicate data points that are off the displayed range. In (b), the SR requirement is indicated by the arrow, and "FNP" represents backgrounds from fake (i.e., misidentified) and non-prompt leptons.

2.3 Run 1 combination

The Run 1 ATLAS $H \to$ inv combination utilised 4.7 fb^{-1} of pp collision data at $\sqrt{s} = 7$ TeV and 20.3 fb^{-1} at $\sqrt{s} = 8$ TeV [36]. This combination considers inputs from direct searches of $H \to$ inv through Higgs bosons produced via VBF or in association with a vector boson V, where the vector boson decays either leptonically ($Z \to \ell\ell$) or hadronically ($W/Z \to jj$). All the signal regions and control regions are used to perform a maximum-likelihood fit resulting in an observed (expected) upper limit of $\mathcal{B}_{H\to\text{inv}} < 0.25$ ($0.27^{+0.10}_{-0.08}$) at the 95% CL. In a similar way to Run 2, the sensitivity is driven by the VBF channel.

3 Statistical model

The statistical combination of the analyses is performed by constructing the product of their likelihoods and maximizing the resulting likelihood ratio [58]:

$$\Lambda(\alpha;\theta) = \frac{L\left(\alpha, \hat{\hat{\theta}}(\alpha)\right)}{L\left(\hat{\alpha}, \hat{\theta}\right)}$$

where α and θ are respectively the parameter of interest and the nuisance parameters. In the numerator, the nuisance parameters are set to their profiled values $\hat{\hat{\theta}}(\alpha)$, which maximise the likelihood function for fixed values of the parameter of interest α. In the denominator, both the parameter of interest and the nuisance parameters are set to the values $\hat{\alpha}$ and $\hat{\theta}$ respectively, which jointly maximise the likelihood. This is done following the implementation described in Ref. [59, 60], with $\mathcal{B}_{H\to\text{inv}}$ as the parameter of interest α. Systematic uncertainties are modelled in the likelihood function as nuisance parameters θ constrained by Gaussian or log-normal probability density functions [36]. Expected results are obtained using the Asimov dataset technique [58]. In absence of a significant excess, upper limits on $\mathcal{B}_{H\to\text{inv}}$ are provided following the CL_s formalism [61] using the profile likelihood ratio as a test statistic. In the following, several combinations will be discussed with an increasing number of input analyses:

1. combination of $t\bar{t}H$-2ℓ and $t\bar{t}H$-0ℓ searches in Run 2
2. combination of $t\bar{t}H$ and VBF searches in Run 2
3. combination of Run 2 and Run 1 results

3.1 Uncertainty correlation in $t\bar{t}H$ combination

The $t\bar{t}H$-0ℓ and $t\bar{t}H$-2ℓ analyses use the same reconstruction and identification for the physics objects, therefore all the experimental systematic uncertainties are treated as correlated. Uncertainties related to the modelling of the $t\bar{t}H$ production are also treated as correlated. The leading background contributions common to the two analyses are $t\bar{t}$ and $t\bar{t}Z$ production. For the former, independent normalisation factors are considered in each analysis and they are constrained in dedicated control regions. As the modelling uncertainties are implemented to cover the extrapolation between the CR and the SR, and the phase space covered by the two analyses is significantly different, such uncertainties are treated as uncorrelated. The $t\bar{t}Z$ process is normalised through a common CR and a single normalisation factor is shared by the two analyses. The $t\bar{t}Z$ modelling uncertainties cover the extrapolation between the CR and the respective SR in the two analyses and they are treated as uncorrelated given the different signal region definitions. Modelling uncertainties for other subdominant backgrounds are treated as uncorrelated.

3.2 Uncertainty correlation in Run 2 combination

In the combination of Run 2 results, the experimental systematic uncertainties related to lepton and photon reconstruction, identification and calibration are correlated across all search channels. Similarly, uncertainties related to the $E_{\text{T}}^{\text{miss}}$, as well as the uncertainty on the integrated luminosity and the modelling of additional pp collisions in the same and neighbouring bunch crossings (pile up) are correlated. The assessment of some of the uncertainties associated to the calibration of the jet energy scale (JES) and the jet energy resolution varies between the different analyses in terms of reconstruction algorithms and parameterisation choices, and are therefore treated as uncorrelated. The impact of this assumption on the final result is estimated using alternative correlation models where each set of systematic uncertainty is treated as correlated or uncorrelated, and found to have an absolute effect on the $\mathcal{B}_{H\to\text{inv}}$ limit of the order of 0.002. Finally, uncertainties related to the flavour tagging of jets have a negligible impact in the VBF analysis and therefore they are only considered for the $t\bar{t}H$ analysis.

The two analyses are dominated by very different background processes; in addition, such backgrounds are normalised in dedicated control regions as close as possible to the respective signal regions. For this reason, any uncertainty related to the background prediction is considered as uncorrelated.

The systematic uncertainties on the total $H \rightarrow$ inv cross section due to the choice of parton distribution functions (PDF) are treated as fully correlated across signal processes in the various analyses. By contrast, uncertainties due to missing higher order QCD corrections and due to parton shower and hadronisation modelling are considered uncorrelated, as their impact on the final discriminants, and thus the result, will in general vary between the different topologies.

3.3 Uncertainty correlation in Run 1 and Run 2 combination

Subsequently, the Run 2 result described above is combined with the Run 1 searches for $H \rightarrow$ inv decays [36]. The adopted correlation scheme follows closely the statistical combination of Run 2 results with the partial dataset with the Run 1 combination [40]. The individual correlation schemes for the two input combinations performed using Run 2 analyses and Run 1 analyses are preserved when including them in the combination across both runs. Due to the differences between the detector layouts and data-taking conditions, reconstruction algorithms and their calibrations, and treatment of systematic uncertainties, the correlations between the runs are not clearly identifiable. Hence, no correlations between Run 1 and 2 are assumed for most instrumental uncertainties. Exceptions are discussed below. The uncertainties related to the modelling of the calorimeter response dependence on jet flavour and pile up are taken as correlated, as they use similar methodology in both runs. Similarly, the calibration of the JES across different η regions of the detector is correlated. The uncertainty on the JES of b-quark jets was estimated using MC simulations [62, 63] and is therefore considered correlated. Background modelling uncertainties are considered to be uncorrelated to reflect improvements in the MC simulation tools that have evolved significantly since Run 1, both on the side of the hard process simulation and on the side of the parton shower and hadronisation models. The impact of these correlation assumptions on the background theory modelling uncertainties is minor given their generally small impact on the final result, due to the extensive use of control regions in the Run 2 VBF analysis. For similar reasons, the signal modelling uncertainties are considered uncorrelated between the runs. All other signal and background modelling uncertainties are considered uncorrelated.

The impact of the correlation assumptions between the runs on the combined $\mathcal{B}_{H\rightarrow\text{inv}}$ limit is estimated by comparing the results obtained with the default correlation scheme discussed above and one where all uncertainties are considered uncorrelated between the runs, and the difference in the expected 95% CL limit is found to be 0.001. In addition, the impact on $\mathcal{B}_{H\rightarrow\text{inv}}$ in scenarios ranging from full anti-correlation to full correlation was studied using the Best Linear Unbiased Estimator (BLUE) [64] for the components of the JES uncertainty, the V+jets background, and diboson production that are nominally not correlated due to different parametrisations in Run 1 and 2, and found to be negligible [40]. This conclusion drawn in the context of the partial Run 2+1 combination applies to this result using the entire Run 2 data given the decreased relative impact of Run 1 results on the combined result.

4 Results

4.1 Combination in the $t\bar{t}H$ topology

The negative logarithmic profile likelihood ratios $-2\,\Delta\ln(\Lambda(\mathcal{B}_{H\to\text{inv}};\theta))$ as a function of $\mathcal{B}_{H\to\text{inv}}$ from the individual analyses and from their combination are shown in Fig. 2 (a). The result of the combination of the $t\bar{t}H$-0ℓ and $t\bar{t}H$-2ℓ analyses is reported in Table 1. The best-fit values of $\mathcal{B}_{H\to\text{inv}}$ from the individual analyses are compatible within one standard deviation. The statistical combination yields a best-fit value of 0.04 ± 0.20. The combined observed upper limit on $\mathcal{B}_{H\to\text{inv}}$ at the 95% CL is 0.40 while the expected value is $0.36^{+0.15}_{-0.10}$. The combination improves the sensitivity of the $t\bar{t}H$-2ℓ analysis by 15%. The overall uncertainty is dominated by the limited number of data events and to a lesser extent by background modelling and JES uncertainties. For further details on the breakdown of systematic uncertainties see Table 3 in the Appendix.

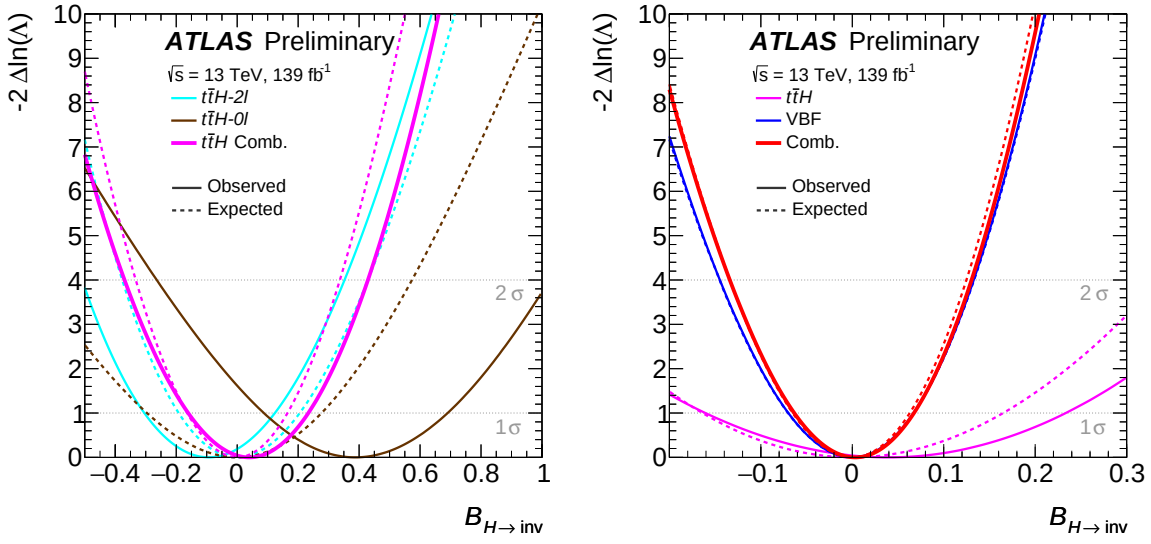

Figure 2: The expected and observed negative logarithmic profile likelihood ratios $-2\,\Delta\ln(\Lambda)$ as a function of $\mathcal{B}_{H\to\text{inv}}$ for the $t\bar{t}H$-0ℓ and $t\bar{t}H$-2ℓ analyses and their statistical combination (a). The expected and observed likelihood profiles for the statistical combination in the $t\bar{t}H$ topology, the $H \to$ inv search in the VBF topology, and their statistical combination (b).

4.2 Combination of Run 2 results

The negative logarithmic profile likelihood ratios $-2\,\Delta\ln(\Lambda(\mathcal{B}_{H\to\text{inv}};\theta))$ as a function of $\mathcal{B}_{H\to\text{inv}}$ from the individual analyses and from the combined Run 2 result are shown in Fig. 2 (b), corresponding to a best-fit combined value of $\mathcal{B}_{H\to\text{inv}} = 0.00^{+0.06}_{-0.07}$.

Overall, the result is dominated by systematic uncertainties. Dominant uncertainties related to the number of simulated MC events, the reconstruction and identification of jets and leptons, and the modelling of background processes other than W/Z + jets production contribute to the total uncertainty at a similar

Table 1: Summary of results from direct searches for invisible decays of the 125 GeV Higgs boson in the $t\bar{t}H$ topology using 139 fb^{-1} of Run 2 data, and their statistical combination. Shown are the best-fit values of $\mathcal{B}_{H\to\text{inv}}$, as well as observed and expected upper limits on $\mathcal{B}_{H\to\text{inv}}$ at the 95% CL. The corresponding Asimov datasets for the expected results are constructed using nuisance parameter values from a fit to data with $\mathcal{B}_{H\to\text{inv}} = 0$, and the quoted uncertainty corresponds to the 68% confidence interval.

Analysis	Best fit $\mathcal{B}_{H\to\text{inv}}$	Observed upper limit	Expected upper limit	Reference
$t\bar{t}H$-0ℓ	0.39 ± 0.30	0.94	$0.64^{+0.29}_{-0.19}$	[44], this document
$t\bar{t}H$-2ℓ	$-0.09^{+0.22}_{-0.21}$	0.37	$0.42^{+0.19}_{-0.12}$	[46], this document
$t\bar{t}H$ comb.	0.04 ± 0.20	0.40	$0.36^{+0.15}_{-0.10}$	This document

level. For further details on the breakdown of systematic uncertainties see Table 4 in the Appendix. In the absence of a significant excess, an upper limit at the 95% CL of $\mathcal{B}_{H\to\text{inv}} < 0.13$ ($0.12^{+0.05}_{-0.04}$) is observed (expected). With respect to the most sensitive single analysis, the VBF Run 2 result, the Run 2 combination brings a relative sensitivity improvement of 5%.

4.3 Combination of Run 1 + Run 2 results

The observed $-2\,\Delta\ln(\Lambda(\mathcal{B}_{H\to\text{inv}};\theta))$ of the combined Run 1+2 result is represented in Fig. 3, alongside the individual Run 1 and Run 2 combinations. A best-fit value of $\mathcal{B}_{H\to\text{inv}} = 0.00 \pm 0.06$ is obtained for the Run 1+2 combination, corresponding to an observed (expected) upper limit of $\mathcal{B}_{H\to\text{inv}} < 0.11$ ($0.11^{+0.04}_{-0.03}$) at the 95% CL. The overall picture of the most relevant sources of uncertainty is very similar to that of the Run 2 combination, with the exception that the relative contribution from the uncertainty on modelling of the W/Z + jets process increases. This is because the Run 1 combination relies heavily on MC simulations of this process due to the limited statistical power of the CRs. For further details on the breakdown of systematic uncertainties see Table 4 in the Appendix. The final result, together with the results in the individual Run 2 analyses as well as the Run-2-only and the Run-1-only combinations, are summarised in Table 2, and the upper limits on $\mathcal{B}_{H\to\text{inv}}$ are graphically represented in Fig. 4. The Run 1+2 combination reaches a relative sensitivity improvement of 15% with respect to the results of the VBF Run 2 analysis, which is the most sensitive input of the combination.

5 Comparison to direct dark matter detection experiments

The constraint from the combined observed (expected) Run 1+2 exclusion limit at 90% CL is $\mathcal{B}_{H\to\text{inv}} < 0.09$ (0.09 ± 0.04). This is compared to the results from representative direct DM detection experiments [65–69] in Fig. 5. This comparison is performed in the context of Higgs portal models [70]. The translation of the $H \to$ inv result into a weakly interacting massive particle (WIMP)-nucleon scattering cross section $\sigma_{\text{WIMP-}N}$ relies on an effective field theory approach [33] under the assumption that Higgs decays to a pair of DM particles are kinematically possible and that the DM particle is a WIMP that is a scalar or a Majorana fermion [23, 71, 72]. In this translation, the nuclear form factor $f_N = 0.308 \pm 0.018$ [73] is used.

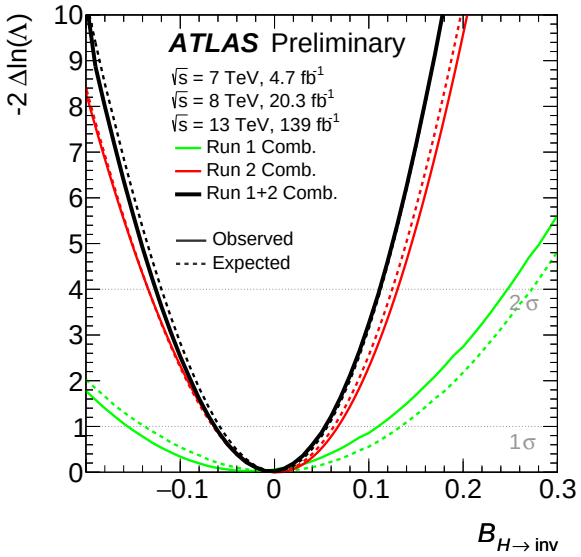

Figure 3: The expected and observed negative logarithmic profile likelihood ratios $-2\,\Delta\ln(\Lambda)$ as a function of $\mathcal{B}_{H\to\text{inv}}$ for the combined results using Run 1 and Run 2 alone, together with their combination.

Table 2: Summary of results from direct searches for invisible decays of the 125 GeV Higgs boson and their statistical combinations. Shown are the best-fit values of $\mathcal{B}_{H\to\text{inv}}$, as well as observed and expected upper limits on $\mathcal{B}_{H\to\text{inv}}$ at the 95% CL. The corresponding Asimov datasets for the expected results are constructed using nuisance parameter values from a fit to data with $\mathcal{B}_{H\to\text{inv}} = 0$, and the quoted uncertainty corresponds to the 68% confidence interval.

Analysis	$\sqrt{s}$ [TeV]	Int. luminosity [fb^{-1}]	Best fit $\mathcal{B}_{H\to\text{inv}}$	Observed upper limit	Expected upper limit	Reference
Run 2 VBF	13	139	$0.00^{+0.07}_{-0.07}$	0.13	$0.13^{+0.05}_{-0.04}$	[42]
Run 2 $t\bar{t}H$	13	139	$0.04^{+0.20}_{-0.20}$	0.40	$0.36^{+0.15}_{-0.10}$	This document
Run 2 Comb.	13	139	$0.00^{+0.06}_{-0.07}$	0.13	$0.12^{+0.05}_{-0.04}$	This document
Run 1 Comb.	7, 8	4.7, 20.3	$-0.02^{+0.14}_{-0.13}$	0.25	$0.27^{+0.10}_{-0.08}$	[36]
Run 1+2 Comb.	7, 8, 13	4.7, 20.3, 139	$0.00^{+0.06}_{-0.06}$	0.11	$0.11^{+0.04}_{-0.03}$	This document

The excluded $\sigma_{\text{WIMP-}N}$ values range down to 10^{-45} cm^2 in the scalar WIMP scenario. In the Majorana fermion WIMP case, the effective coupling is reduced by m_H^2 [33], excluding $\sigma_{\text{WIMP-}N}$ values down to 2×10^{-47} cm^2.

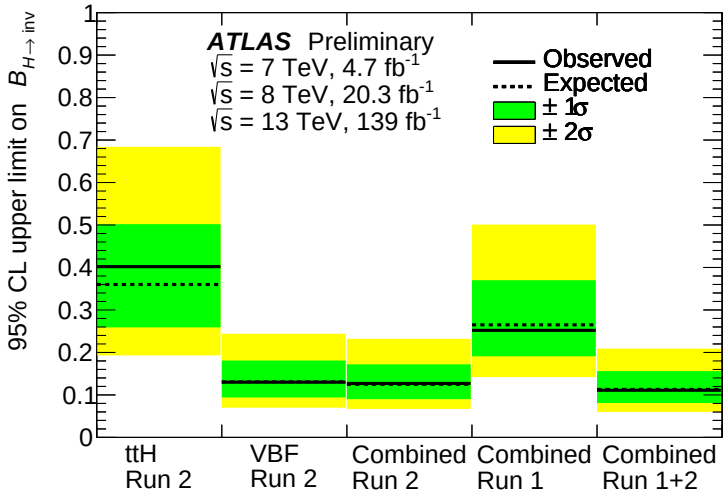

Figure 4: The observed and expected upper limits on $\mathcal{B}_{H\to\text{inv}}$ at the 95% CL from direct searches for invisible decays of the 125 GeV Higgs boson and their statistical combinations in Run 1 and 2. The 1σ and 2σ uncertainty bands on the expected limits are shown as green and yellow, respectively.

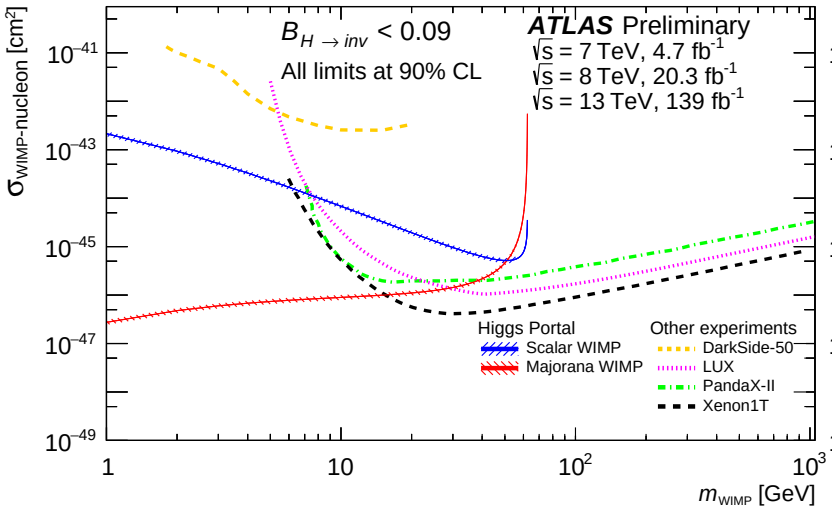

Figure 5: Comparison of the upper limits at 90% CL from direct detection experiments [66–69] on the spin-independent WIMP-nucleon scattering cross section to the observed exclusion limits from this analysis, as a function of the WIMP mass. The interpretation of ATLAS results assumes Higgs portal scenarios where the 125 GeV Higgs boson decays to a pair of DM particles [33, 70] that are either scalars or Majorana fermions. The uncertainties from the nuclear form factor are indicated by the hatched band. The regions above the limit contours are excluded in the $\sigma_{\text{WIMP-}N}$ range shown in the plot.

6 Conclusion

In summary, direct searches for invisible Higgs boson decays using 139 fb^{-1} of pp collision data at $\sqrt{s}$ = 13 TeV recorded in Run 2 of the LHC in the VBF and $t\bar{t}H$ topologies are statistically combined

assuming Higgs boson production according to the SM. An upper limit on the invisible Higgs boson branching ratio of $\mathcal{B}_{H\to\text{inv}} < 0.13$ ($0.12^{+0.05}_{-0.04}$) is observed (expected) at the 95% CL. A statistical combination of this result with the combination of direct $H \to$ inv searches using up to 4.7 fb^{-1} of pp collision data at $\sqrt{s} = 7$ TeV and up to 20.3 fb^{-1} at 8 TeV collected in Run 1 of the LHC yields an observed (expected) upper limit of $\mathcal{B}_{H\to\text{inv}} < 0.11$ ($0.11^{+0.04}_{-0.03}$) at the 95% CL. The combined Run 1+2 result is translated into upper limits on the WIMP-nucleon scattering cross section for Higgs portal models. The derived limits on $\sigma_{\text{WIMP-}N}$ range down to 10^{-45} cm^2 and 2×10^{-47} cm^2 in the scalar and Majorana fermion WIMP scenarios, respectively, highlighting the complementarity of DM searches at the LHC and direct detection experiments.

Appendix

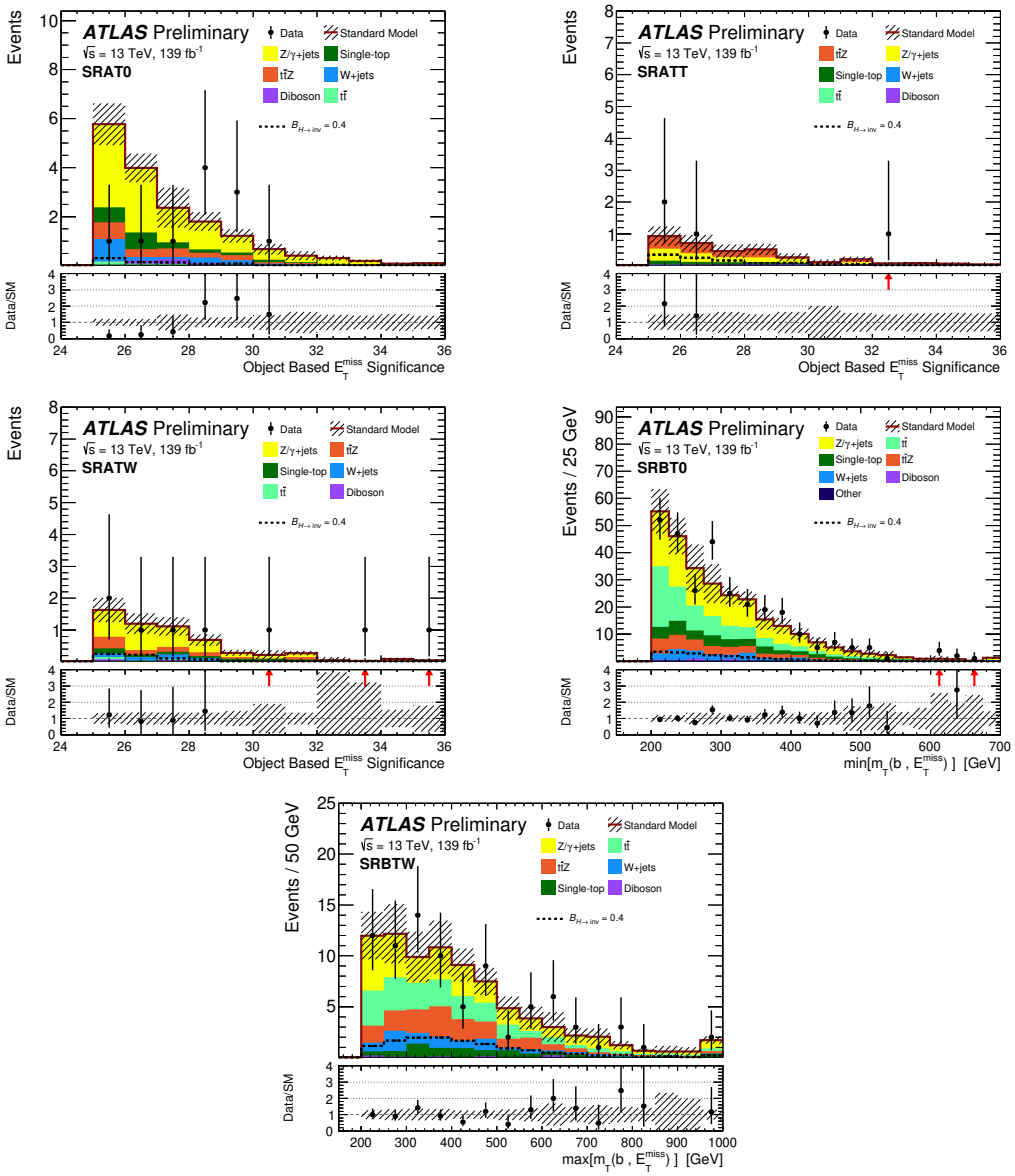

Figure 6: Distributions of the main discriminating variables in the $t\bar{t}H$-0ℓ channel SRs [44]. The two sets of SRs, SRA and SRB are differentiated, among other selections, by requiring events with m_{T2} greater or less than 450 GeV respectively. Each of these regions is broken down further into three categories defined by the mass of the reclustered large-radius ($R = 1.2$) jet of the sub-leading top quark candidate: $m_2^{R=1.2} < 60$ GeV (T0), $60 < m_2^{R=1.2} < 120$ GeV (TW), and $m_2^{R=1.2} > 120$ GeV (TT). The contributions from all the backgrounds are shown as stacked histograms, with the hashed bands representing the total uncertainty. The expected distributions for the $H \rightarrow$ inv signal are overlaid as dashed lines. Red arrows in the ratio panel indicate data points that are off the displayed range.

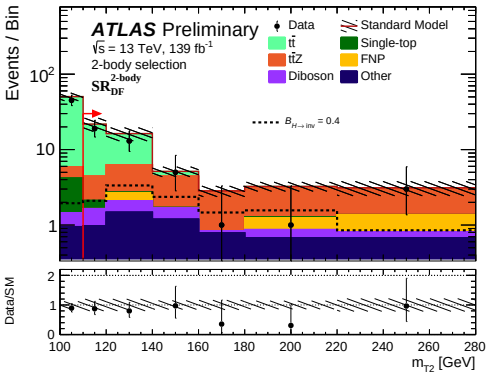

Figure 7: m_{T2} distribution for the different-flavour events selected in the $t\bar{t}H$-2ℓ channel [46]. The SR requirement over the plotted variable is indicated by the arrow. The contributions from all the backgrounds are shown as stacked histograms, with the hashed bands representing the total uncertainty. The expected distributions for the $H \rightarrow$ inv signal are overlaid as dashed lines.

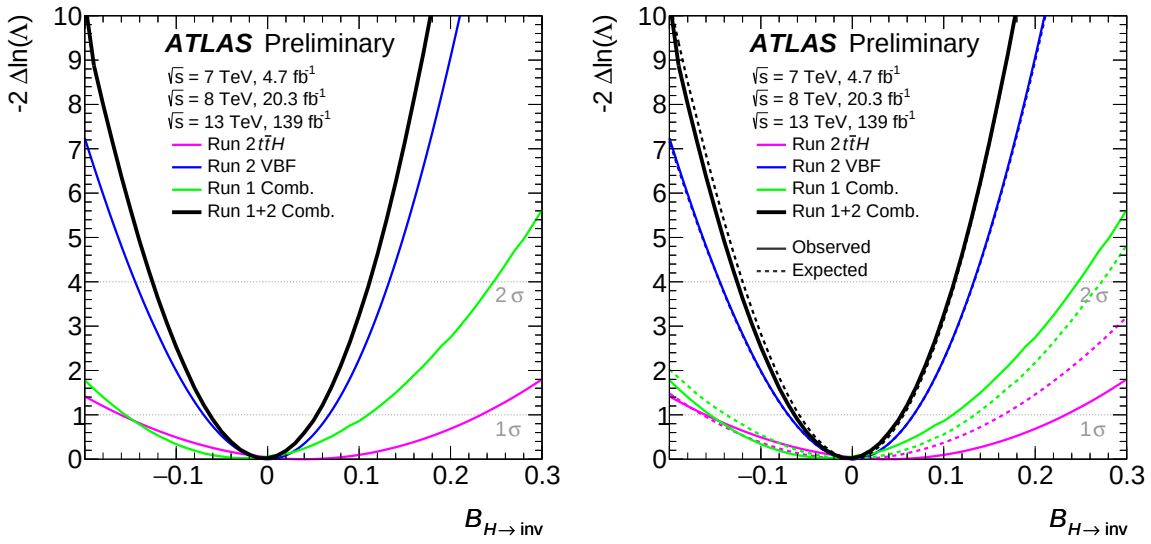

(a) (b)

Figure 8: The observed negative logarithmic profile likelihood ratios $-2\,\Delta\ln(\Lambda)$ as a function of $\mathcal{B}_{H\rightarrow\mathrm{inv}}$ for the different input analyses and their combinations (a). The same distributions including the expected curves are shown in (b).

Table 3: The expected impact of different categories of systematic uncertainty on $\mathcal{B}_{H\to\text{inv}}$ in the $t\bar{t}H$-0ℓ and $t\bar{t}H$-2ℓ combination. The evaluation is performed by ignoring a given category of systematic uncertainties and quadratically subtracting the changed uncertainty on the expected best-fit $\mathcal{B}_{H\to\text{inv}}$ value from the nominal case with the full uncertainty treatment. Due to residual correlations between categories, the quadratic sum of systematic uncertainties can differ from the actual number. The uncertainty due to finite number of data events ("data statistical uncertainty") is obtained by ignoring all systematic uncertainties and the floating background normalisations. The sum of all systematic uncertainties is estimated by quadratically subtracting the above uncertainty and the one from floating background normalisations from the total uncertainty. The experimental uncertainty and the uncertainty related to the size of the MC sample ("MC statistical uncertainty") are treated as separate categories. The uncertainties are reported as the upper part of the 68% confidence interval on the expected best-fit $\mathcal{B}_{H\to\text{inv}}$ value. The corresponding Asimov datasets are constructed using nuisance parameter values from a fit to data with $\mathcal{B}_{H\to\text{inv}} = 0$.

Source of uncertainty	±Uncertainty on $\mathcal{B}_{H\to\text{inv}}$ $t\bar{t}H$
Luminosity / pile up	0.006
Leptons / photons	0.025
Jets	0.036
Flavour tagging	0.019
$E_{\text{T}}^{\text{miss}}$	0.013
$t\bar{t}$ modelling	0.055
$t\bar{t}$ + Z modelling	0.035
Other background modelling	0.047
Data-driven background	0.003
Signal modelling	0.015
MC statistical uncertainty	0.009
All experimental	0.053
All theory	0.080
Total systematic uncertainty	0.099
Data statistical uncertainty	0.116
Floating background norm.	0.064
Total statistical uncertainty	0.132
Total uncertainty	0.165

Table 4: The expected impact of different categories of systematic uncertainty on $\mathcal{B}_{H\to\text{inv}}$ in the Run 2 and Run 1+2 combinations. The evaluation is performed by ignoring a given category of systematic uncertainties and quadratically subtracting the changed uncertainty on the expected best-fit $\mathcal{B}_{H\to\text{inv}}$ value from the nominal case with the full uncertainty treatment. Due to residual correlations between categories, the quadratic sum of systematic uncertainties can differ from the actual number. The uncertainty due to finite number of data events ("data statistical uncertainty") is obtained by ignoring all systematic uncertainties and the floating background normalisations. The sum of all systematic uncertainties is estimated by quadratically subtracting the above uncertainty and the one from floating background normalisations from the total uncertainty. The experimental uncertainty and the uncertainty related to the size of the MC sample ("MC statistical uncertainty") are treated as separate categories. The uncertainties are reported as the upper part of the 68% confidence interval on the expected best-fit $\mathcal{B}_{H\to\text{inv}}$ value. The corresponding Asimov datasets are constructed using nuisance parameter values from a fit to data with $\mathcal{B}_{H\to\text{inv}} = 0$.

Source of uncertainty	±Uncertainty on $\mathcal{B}_{H\to\text{inv}}$	
	Run 2	Run 1+2
Luminosity / pile up	0.002	0.003
Leptons / photons	0.018	0.015
Jets	0.023	0.019
Flavour tagging	0.002	0.002
$E_{\text{T}}^{\text{miss}}$	0.008	0.007
V+jets modelling	0.011	0.017
Other background modelling	0.015	0.015
Data-driven background	0.023	0.019
Signal modelling	0.004	0.003
MC statistical uncertainty	0.023	0.021
All experimental	0.041	0.036
All theory	0.030	0.030
Total systematic uncertainty	0.051	0.046
Data statistical uncertainty	0.019	0.018
Floating background norm.	0.031	0.028
Total statistical uncertainty	0.037	0.034
Total uncertainty	0.063	0.057

Table 5: Summary of results from direct searches for invisible decays of the 125 GeV Higgs boson and their statistical combinations. Shown are the observed and expected upper limits on $\mathcal{B}_{H\to\text{inv}}$ at the 90% CL. The corresponding Asimov datasets for the expected results are constructed using nuisance parameter values from a fit to data with $\mathcal{B}_{H\to\text{inv}} = 0$, and the quoted uncertainty corresponds to the 68% confidence interval.

Analysis	$\sqrt{s}$ [TeV]	Int. luminosity [fb^{-1}]	Observed upper limit at the 90% CL	Expected upper limit at the 90% CL	Reference
Run 2 VBF	13	139	0.11	$(0.11^{+0.05}_{-0.05})$	[42]
Run 2 ttH	13	139	0.34	$(0.30^{+0.14}_{-0.12})$	This document
Run 2 comb.	13	139	0.11	$(0.10^{+0.04}_{-0.04})$	This document
Run 1 comb.	7, 8	4.7, 20.3	0.21	$(0.22^{+0.10}_{-0.08})$	[36]
Run 1+2 comb.	7, 8, 13	4.7, 20.3, 139	0.09	$(0.09^{+0.04}_{-0.04})$	This document

References

[1] Y. Akrami et al., *Planck 2018 results. I. Overview and the cosmological legacy of Planck*, Astron. Astrophys. **641** (2020) A1, arXiv: 1807.06205 [astro-ph.CO] (cit. on p. 2).

[2] WMAP Collaboration, *Nine-Year Wilkinson Microwave Anisotropy Probe (WMAP) Observations: Cosmological Parameter Results*, Astrophys. J. Suppl. **208** (2013) 19, arXiv: 1212.5226 [astro-ph.CO] (cit. on p. 2).

[3] G. Bertone, D. Hooper and J. Silk, *Particle dark matter: Evidence, candidates and constraints*, Phys. Rept. **405** (2005) 279, arXiv: hep-ph/0404175 (cit. on p. 2).

[4] V. Trimble, *Existence and Nature of Dark Matter in the Universe*, Ann. Rev. Astron. Astrophys. **25** (1987) 425 (cit. on p. 2).

[5] H. Goldberg, *Constraint on the Photino Mass from Cosmology*, Phys. Rev. Lett. **50** (1983) 1419, Erratum: Phys. Rev. Lett. **103** (2009) 099905 (cit. on p. 2).

[6] J. R. Ellis, J. S. Hagelin, D. V. Nanopoulos, K. A. Olive and M. Srednicki, *Supersymmetric Relics from the Big Bang*, Nucl. Phys. B **238** (1984) 453 (cit. on p. 2).

[7] G. Jungman, M. Kamionkowski and K. Griest, *Supersymmetric dark matter*, Phys. Rept. **267** (1996) 195, arXiv: hep-ph/9506380 (cit. on p. 2).

[8] G. Steigman and M. S. Turner, *Cosmological constraints on the properties of weakly interacting massive particles*, Nucl. Phys. B **253** (1985) 375 (cit. on p. 2).

[9] R. J. Scherrer and M. S. Turner, *On the relic, cosmic abundance of stable, weakly interacting massive particles*, Phys. Rev. D **33** (1986) 1585, [Erratum: Phys. Rev. D **34** (1986) 3263] (cit. on p. 2).

[10] D. Abercrombie et al., *Dark Matter Benchmark Models for Early LHC Run-2 Searches: Report of the ATLAS/CMS Dark Matter Forum*, (2015), arXiv: 1507.00966 [hep-ex] (cit. on p. 2).

[11] J. L. Feng, *Dark Matter Candidates from Particle Physics and Methods of Detection*, Ann. Rev. Astron. Astrophys. **48** (2010) 495, arXiv: 1003.0904 [astro-ph.CO] (cit. on p. 2).

[12] A. Boveia and C. Doglioni, *Dark Matter Searches at Colliders*, Ann. Rev. Nucl. Part. Sci. **68** (2018) 429, arXiv: 1810.12238 [hep-ex] (cit. on p. 2).

[13] ATLAS Collaboration, *Observation of a new particle in the search for the Standard Model Higgs boson with the ATLAS detector at the LHC*, Phys. Lett. B **716** (2012) 1, arXiv: 1207.7214 [hep-ex] (cit. on p. 2).

[14] CMS Collaboration, *Observation of a new boson at a mass of 125 GeV with the CMS experiment at the LHC*, Phys. Lett. B **716** (2012) 30, arXiv: 1207.7235 [hep-ex] (cit. on p. 2).

[15] I. Antoniadis, M. Tuckmantel and F. Zwirner, *Phenomenology of a leptonic goldstino and invisible Higgs boson decays*, Nucl. Phys. **707** (2005) 215, arXiv: hep-ph/0410165 [hep-ph] (cit. on p. 2).

[16] N. Arkani-Hamed, S. Dimopoulos, G. R. Dvali and J. March-Russell, *Neutrino masses from large extra dimensions*, Phys. Rev. D **65** (2001) 024032, arXiv: hep-ph/9811448 [hep-ph] (cit. on p. 2).

[17] A. Datta, K. Huitu, J. Laamanen and B. Mukhopadhyaya, *Linear collider signals of an invisible Higgs boson in theories of large extra dimensions*, Phys. Rev. D **70** (2004) 075003, arXiv: hep-ph/0404056 [hep-ph] (cit. on p. 2).

[18] S. Kanemura, S. Matsumoto, T. Nabeshima and N. Okada, *Can WIMP dark matter overcome the nightmare scenario?*, Phys. Rev. D **82** (2010) 055026, arXiv: 1005.5651 [hep-ph] (cit. on p. 2).

[19] A. Djouadi, O. Lebedev, Y. Mambrini and J. Quevillon, *Implications of LHC searches for Higgs–portal dark matter*, Phys. Lett. B **709** (2012) 65, arXiv: 1112.3299 [hep-ph] (cit. on p. 2).

[20] A. Djouadi, A. Falkowski, Y. Mambrini and J. Quevillon, *Direct detection of Higgs-portal dark matter at the LHC*, Eur. Phys. J. C **73** (2013) 2455, arXiv: 1205.3169 [hep-ph] (cit. on p. 2).

[21] R. E. Shrock and M. Suzuki, *Invisible Decays of Higgs Bosons*, Phys. Lett. B **110** (1982) 250 (cit. on p. 2).

[22] D. Choudhury and D. P. Roy, *Signatures of an invisibly decaying Higgs particle at LHC*, Phys. Lett. B **322** (1994) 368, arXiv: hep-ph/9312347 [hep-ph] (cit. on p. 2).

[23] O. J. P. Eboli and D. Zeppenfeld, *Observing an invisible Higgs boson*, Phys. Lett. B **495** (2000) 147, arXiv: hep-ph/0009158 [hep-ph] (cit. on pp. 2, 9).

[24] H. Davoudiasl, T. Han and H. E. Logan, *Discovering an invisibly decaying Higgs at hadron colliders*, Phys. Rev. D **71** (2005) 115007, arXiv: hep-ph/0412269 [hep-ph] (cit. on p. 2).

[25] R. M. Godbole, M. Guchait, K. Mazumdar, S. Moretti and D. P. Roy, *Search for 'invisible' Higgs signals at LHC via associated production with gauge bosons*, Phys. Lett. B **571** (2003) 184, arXiv: hep-ph/0304137 [hep-ph] (cit. on p. 2).

[26] D. Ghosh, R. Godbole, M. Guchait, K. Mohan and D. Sengupta, *Looking for an Invisible Higgs Signal at the LHC*, Phys. Lett. B **725** (2013) 344, arXiv: 1211.7015 [hep-ph] (cit. on p. 2).

[27] G. Belanger, B. Dumont, U. Ellwanger, J. F. Gunion and S. Kraml, *Status of invisible Higgs decays*, Phys. Lett. B **723** (2013) 340, arXiv: 1302.5694 [hep-ph] (cit. on p. 2).

[28] D. Curtin et al., *Exotic decays of the 125 GeV Higgs boson*, Phys. Rev. D **90** (2014) 075004, arXiv: 1312.4992 [hep-ph] (cit. on p. 2).

[29] D. de Florian et al., *Handbook of LHC Higgs Cross Sections: 4. Deciphering the Nature of the Higgs Sector*, **2/2017** (2016), arXiv: 1610.07922 [hep-ph] (cit. on p. 2).

[30] ATLAS Collaboration, *The ATLAS Experiment at the CERN Large Hadron Collider*, JINST **3** (2008) S08003 (cit. on pp. 2, 3).

[31] ATLAS Collaboration, *ATLAS Insertable B-Layer Technical Design Report*, ATLAS-TDR-19 (2010), URL: http://cds.cern.ch/record/1291633, ATLAS Insertable B-Layer Technical Design Report Addendum, ATLAS-TDR-19-ADD-1 (2012), URL: http://cds.cern.ch/record/1451888 (cit. on pp. 2, 3).

[32] B. Abbott et al., *Production and Integration of the ATLAS Insertable B-Layer*, JINST **13** (2018) T05008, arXiv: 1803.00844 [physics.ins-det] (cit. on p. 2).

[33] ATLAS Collaboration, *Search for invisible decays of a Higgs boson using vector-boson fusion in pp collisions at $\sqrt{s} = 8$ TeV with the ATLAS detector*, JHEP **01** (2016) 172, arXiv: 1508.07869 [hep-ex] (cit. on pp. 2, 9–11).

[34] ATLAS Collaboration, *Search for Invisible Decays of a Higgs Boson Produced in Association with a Z Boson in ATLAS*, Phys. Rev. Lett. **112** (2014) 201802, arXiv: 1402.3244 [hep-ex] (cit. on p. 2).

[35] ATLAS Collaboration, *Search for invisible decays of the Higgs boson produced in association with a hadronically decaying vector boson in pp collisions at $\sqrt{s} = 8$ TeV with the ATLAS detector*, Eur. Phys. J. C **75** (2015) 337, arXiv: 1504.04324 [hep-ex] (cit. on p. 2).

[36] ATLAS Collaboration, *Constraints on new phenomena via Higgs boson couplings and invisible decays with the ATLAS detector*, JHEP **11** (2015) 206, arXiv: 1509.00672 [hep-ex] (cit. on pp. 2, 3, 5–7, 10, 17).

[37] ATLAS Collaboration, *Search for invisible Higgs boson decays in vector boson fusion at $\sqrt{s}$ = 13 TeV with the ATLAS detector*, Phys. Lett. B **793** (2019) 499, arXiv: 1809.06682 [hep-ex] (cit. on p. 2).

[38] ATLAS Collaboration, *Search for an invisibly decaying Higgs boson or dark matter candidates produced in association with a Z boson in pp collisions at $\sqrt{s}$ = 13 TeV with the ATLAS detector*, Phys. Lett. B **776** (2018) 318, arXiv: 1708.09624 [hep-ex] (cit. on p. 2).

[39] ATLAS Collaboration, *Search for dark matter in events with a hadronically decaying vector boson and missing transverse momentum in pp collisions at $\sqrt{s}$ = 13 TeV with the ATLAS detector*, JHEP **10** (2018) 180, arXiv: 1807.11471 [hep-ex] (cit. on p. 2).

[40] ATLAS Collaboration, *Combination of Searches for Invisible Higgs Boson Decays with the ATLAS Experiment*, Phys. Rev. Lett. **122** (2019) 231801, arXiv: 1904.05105 [hep-ex] (cit. on pp. 2, 7).

[41] ATLAS Collaboration, *Combined measurements of Higgs boson production and decay using up to 80 fb^{-1} of proton–proton collision data at $\sqrt{s}$ = 13 TeV collected with the ATLAS experiment*, Phys. Rev. D **101** (2020) 012002, arXiv: 1909.02845 [hep-ex] (cit. on p. 2).

[42] ATLAS Collaboration, *Search for invisible Higgs boson decays with vector boson fusion signatures with the ATLAS detector using an integrated luminosity of 139 fb^{-1}*, ATLAS-CONF-2020-008, 2020, URL: https://cds.cern.ch/record/2715447 (cit. on pp. 2, 3, 10, 17).

[43] ATLAS Collaboration, *Search for new phenomena in events with jets and missing transverse momentum in p p collisions at $\sqrt{s}$ = 13 TeV with the ATLAS detector*, ATLAS-CONF-2020-048, 2020, URL: https://cds.cern.ch/record/2728058 (cit. on p. 2).

[44] ATLAS Collaboration, *Search for a scalar partner of the top quark in the all-hadronic $t\bar{t}$ plus missing transverse momentum final state at $\sqrt{s}$ = 13 TeV with the ATLAS detector*, Eur. Phys. J. C **80** (2020) 737, arXiv: 2004.14060 [hep-ex] (cit. on pp. 2–4, 9, 13).

[45] ATLAS Collaboration, *Search for new phenomena with top quark pairs in final states with one lepton, jets, and missing transverse momentum in pp collisions at $\sqrt{s}$ = 13 TeV with the ATLAS detector*, ATLAS-CONF-2020-003, 2020, URL: https://cds.cern.ch/record/2711489 (cit. on p. 2).

[46] ATLAS Collaboration, *Search for new phenomena in events with two opposite-charge leptons, jets and missing transverse momentum in pp collisions at $\sqrt{s}$ = 13 TeV with the ATLAS detector*, ATLAS-CONF-2020-046, 2020, URL: https://cds.cern.ch/record/2728056 (cit. on pp. 2–4, 9, 14).

[47] ATLAS Collaboration, *A combination of measurements of Higgs boson production and decay using up to 139 fb^{-1} of proton–proton collision data at $\sqrt{s}$ = 13 TeV collected with the ATLAS experiment*, ATLAS-CONF-2020-027, 2020, URL: https://cds.cern.ch/record/2725733 (cit. on p. 2).

[48] A. M. Sirunyan et al., *Search for dark matter produced in association with a leptonically decaying Z boson in proton-proton collisions at $\sqrt{s}$ = 13 TeV*, (2020), arXiv: 2008.04735 [hep-ex] (cit. on p. 2).

[49] CMS Collaboration, *Search for invisible decays of a Higgs boson produced through vector boson fusion in proton–proton collisions at $\sqrt{s}$ = 13 TeV*, Phys. Lett. B **793** (2019) 520, arXiv: 1809.05937 [hep-ex] (cit. on p. 2).

[50] A. M. Sirunyan et al., *Search for dark matter particles produced in association with a top quark pair at $\sqrt{s}$ = 13 TeV*, Phys. Rev. Lett. **122** (2019) 011803, arXiv: 1807.06522 [hep-ex] (cit. on p. 2).

[51] CMS Collaboration, *Search for new physics in events with a leptonically decaying Z boson and a large transverse momentum imbalance in proton–proton collisions at $\sqrt{s}$ = 13 TeV*, Eur. Phys. J. C **78** (2018) 291, arXiv: 1711.00431 [hep-ex] (cit. on p. 2).

[52] CMS Collaboration, *Search for new physics in final states with an energetic jet or a hadronically decaying W or Z boson and transverse momentum imbalance at* $\sqrt{s} = 13$ TeV, Phys. Rev. D **97** (2018) 092005, arXiv: 1712.02345 [hep-ex] (cit. on p. 2).

[53] CMS Collaboration, *Searches for invisible decays of the Higgs boson in pp collisions at* $\sqrt{s} = 7$, *8, and 13 TeV*, JHEP **02** (2017) 135, arXiv: 1610.09218 [hep-ex] (cit. on p. 2).

[54] CMS Collaboration, *Search for invisible decays of Higgs bosons in the vector boson fusion and associated ZH production modes*, Eur. Phys. J. C **74** (2014) 2980, arXiv: 1404.1344 [hep-ex] (cit. on p. 2).

[55] ATLAS Collaboration, *Object-based missing transverse momentum significance in the ATLAS Detector*, ATLAS-CONF-2018-038, 2018, URL: https://cds.cern.ch/record/2630948 (cit. on p. 4).

[56] A. Barr, C. Lester and P. Stephens, *m(T2) : The Truth behind the glamour*, J. Phys. G **29** (2003) 2343, arXiv: hep-ph/0304226 (cit. on p. 4).

[57] C. G. Lester and D. J. Summers, *Measuring masses of semiinvisibly decaying particles pair produced at hadron colliders*, Phys. Lett. B **463** (1999) 99, arXiv: hep-ph/9906349 (cit. on p. 4).

[58] G. Cowan et al., *Asymptotic formulae for likelihood-based tests of new physics*, Eur. Phys. J. C **71** (2011) 1554, [Erratum: Eur. Phys. J. C **73** (2013) 2501], arXiv: 1007.1727 [physics.data-an] (cit. on pp. 5, 6).

[59] W. Verkerke and D. P. Kirkby, *The RooFit toolkit for data modeling*, eConf **C0303241** (2003) MOLT007, arXiv: physics/0306116 [physics] (cit. on p. 6).

[60] L. Moneta et al., *The RooStats Project*, (2010), arXiv: 1009.1003 [physics.data-an] (cit. on p. 6).

[61] A. L. Read, *Presentation of search results: the* CL_s *technique*, J. Phys. G **28** (2002) 2693 (cit. on p. 6).

[62] ATLAS Collaboration, *Jet energy measurement and its systematic uncertainty in proton–proton collisions at* $\sqrt{s} = 7$ *TeV with the ATLAS detector*, Eur. Phys. J. C **75** (2015) 17, arXiv: 1406.0076 [hep-ex] (cit. on p. 7).

[63] ATLAS Collaboration, *Jet energy scale measurements and their systematic uncertainties in proton–proton collisions at* $\sqrt{s} = 13$ *TeV with the ATLAS detector*, Phys. Rev. D **96** (2017) 072002, arXiv: 1703.09665 [hep-ex] (cit. on p. 7).

[64] L. Lyons, D. Gibaut and P. Clifford, *How to Combine Correlated Estimates of a Single Physical Quantity*, Nucl. Instrum. Meth. **A270** (1988) 110 (cit. on p. 7).

[65] F. Petricca et al. (CRESST Collaboration), 'First results on low-mass dark matter from the CRESST-III experiment', *15th International Conference on Topics in Astroparticle and Underground Physics (TAUP 2017) Sudbury, Ontario, Canada, July 24-28, 2017*, 2017, arXiv: 1711.07692 [astro-ph.CO] (cit. on p. 9).

[66] D. Akerib, et al. (LUX Collaboration), *Results from a search for dark matter in the complete LUX exposure*, Phys. Rev. Lett. **118** (2017) 021303, arXiv: 1608.07648 [astro-ph.CO] (cit. on pp. 9, 11).

[67] X. Cui et al. (PandaX-II Collaboration), *Dark Matter Results From 54-Ton-Day Exposure of PandaX-II Experiment*, Phys. Rev. Lett. **119** (2017) 181302, arXiv: 1708.06917 [astro-ph.CO] (cit. on pp. 9, 11).

[68] E. Aprile et al. (XENON Collaboration), *Dark Matter Search Results from a One Ton-Year Exposure of XENON1T*, Phys. Rev. Lett. **121** (2018) 111302, arXiv: 1805.12562 [astro-ph.CO] (cit. on pp. 9, 11).

[69] P. Agnes et al. (DarkSide Collaboration), *Low-Mass Dark Matter Search with the DarkSide-50 Experiment*, Phys. Rev. Lett. **121** (2018) 081307, arXiv: 1802.06994 [astro-ph.HE] (cit. on pp. 9, 11).

[70] B. Patt and F. Wilczek, *Higgs-field portal into hidden sectors*, (2006), arXiv: hep-ph/0605188 [hep-ph] (cit. on pp. 9, 11).

[71] P. J. Fox, R. Harnik, J. Kopp and Y. Tsai, *Missing Energy Signatures of Dark Matter at the LHC*, Phys. Rev. D **85** (2012) 056011, arXiv: 1109.4398 [hep-ph] (cit. on p. 9).

[72] A. De Simone, G. F. Giudice and A. Strumia, *Benchmarks for Dark Matter Searches at the LHC*, JHEP **06** (2014) 081, arXiv: 1402.6287 [hep-ph] (cit. on p. 9).

[73] M. Hoferichter, P. Klos, J. Menéndez and A. Schwenk, *Improved Limits for Higgs-Portal Dark Matter from LHC Searches*, Phys. Rev. Lett. **119** (2017) 181803, arXiv: 1708.02245 [hep-ph] (cit. on p. 9).